Mechanics & Industry **20**, 507 (2019)
© AFM, EDP Sciences 2019
https://doi.org/10.1051/meca/2019032

Mechanics & Industry

Available online at:
www.mechanics-industry.org

REGULAR ARTICLE

Numerical and experimental investigation on the effect of the two-phase flow pattern on heat transfer of piston cooling gallery

Lijun Deng*, Jian Zhang, Guannan Hao, and Jing Liu

College of Electromechanical Engineering, Binzhou University, Binzhou 256600, Shandong, PR China

Received: 15 August 2018 / Accepted: 15 April 2019

Abstract. To study factors affecting the formation and conversion of two-phase flow pattern as well as the heat transfer of piston cooling gallery, a transient visual target test bench was set up to research the oscillatory flow characteristics in the cooling gallery under idle condition of the engine. The computational fluid dynamics (CFD) was employed while dynamic mesh technology, SST k–ω turbulence model and volume of fluid (VOF) two-phase flow model were applied to simulate the flow process of piston cooling gallery so as to predict the distribution pattern of two-phase flow. Simulation results were in good agreement with that experimentally obtained. It was observed that in the reciprocating movement of the piston, the action of two-phase flow oscillation was severe, forming some unstable wave flows and slug flows. Results show that under the same pipe diameter, the increase of fluid viscosity results in the decrease of amplitude and the increase of the liquid slugs number as well as the enhancement on heat transfer effect. In addition, it was revealed that injection pressure has little effect on the two-phase flow pattern. However, when the pressure is reduced, the change of the liquid phase is weakened and the locations of flow pattern transition move towards to the behind, thus the impact on the heat transfer is also faint.

Keywords: Two-phase flow / computational fluid dynamics / piston cooling gallery / flow pattern

1 Introduction

With the continuous improvement of emission standards for combustion engines, thermal load of pistons has become a prominent issue which dominates the structural strengthening of engines. As the primary structure in the heat transfer enhancement of pistons, the cooling gallery is expected to be well designed. As reported in published literature [1–3], coolant in an appropriately designed cooling gallery can carry off 50% of the heat.

The two-phase flow and heat transfer mechanism in cooling gallery have been widely investigated. Earlier studies focused on observations through experiments. For instance, Torregrosa et al. [4,5] established a static injection test bench where the heat transfer process in piston cooling gallery was conducted by using the oil heating device and the piston oil temperature control system. It was revealed that the heat transfer in cooling gallery is mainly dependent on the relative distance between the Reynolds number, the Prandtl number and the piston cooling nozzle and the piston cooling gallery inlet. With the diversification of research methods, more scholars tried to study the cooling gallery by different ways, wherein the visualization experiment is one of them. However, it was difficult to obtain the visualization of the internal oil flow state and the heat transfer characteristic with the change of the crank angle, because of the slender profile and complicated structure of the cooling gallery. Therefore, most scholars have simplified the test bench. Evans and Cocktail [6] visualized the open cooling gallery and used the numerical calculation method to obtain the average heat transfer coefficient for both inner and outer cooling galleries. Pimenta and Filho [7] discussed the oil circulation during the piston cycle and used the finite element analysis method to extend Evans' piston cavity jet model so as to evaluate the temperature distribution and heat flux of the piston. Nozawa et al. [8,9] developed a special device to visually observe the oil movement and to measure the oil flow and heat transfer rate in an internal cooling gallery.

In recent years, computational fluid dynamics (CFD) has become the primary means of studying fluid flow through which the correlation between the flow and the heat transfer in the cooling gallery is investigated, and dominant factors affecting the heat transfer are also identified. Kajiwara et al. [10,11] studied the heat transfer in two-dimensional cavity by numerical method. The heat

* e-mail: denglijun_piston@163.com

transfer coefficient of the cooling gallery was determined, and the temperature of the cooling gallery and the temperature distribution of the entire piston head were predicted by reciprocating motion. Fu et al. [12] simplified the three-dimensional cooling gallery into a "Π" shaped and two-dimensional channel, which is transformed into a dynamic boundary problem, where the finite element method and Lagrangian dynamics method were employed to study the oscillation frequency, amplitude and the Reynolds number on the heat transfer rate of the piston cooling. Pan et al. [13] studied the oscillation characteristics of the cooling gallery in both two-dimensional and three-dimensional models and simulated the heat transfer of the cooling gallery during the whole injection process at different crank angles, obtaining the distribution and filling rate of the oil with respect to crank angle which provides the foundation for further study on the effect of the filling rate on the heat transfer coefficient. Yong et al. [14] used the multiphase flow model to simulate the flow and heat transfer in the cooling gallery, and combined with the experiment to verify the accuracy of the numerical model for predicting the oscillation heat transfer in the cooling gallery.

The crucial problems, including the distinction and identification of flow pattern, the description of flow state, need to be solved in the study of fluid heat transfer in the cooling gallery. As various factors affect the flow pattern, each flow pattern has its specific two-phase distribution and interface shape. The change of the flow pattern of the gas-liquid two-phase flow in the cooling gallery is a complicated process, and the interface shape changes with the position, engine speed and pressure of the piston, resulting in the change of the flow pattern. The formation and transition of two-phase flow patterns is an important factor affecting flow and the heat transfer [15]. Several factors influencing the heat transfer performance, such as the movement conditions of the air-oil two-phase flow inside the gallery, the instantaneous oil distributions, the relative oil velocity, the instantaneous acceleration and the velocity of the piston, were investigated by Deng et al. [16]. For two-phase flow, Wang's team [17–19] studied the dynamic flow characteristics and the transition mechanism of the flow pattern in detail, based on the theories of dynamic fluctuation and system identification and technologies of data processing and data acquisition. Subsequently, Wang and coworkers and Lv and coworkers [20–22] simplified the model, taking piston cooling gallery as the research object, and used the high-speed camera to capture the flow pattern when the crank angle varied. The effects of oscillation frequency, gas content and two-phase distribution on the turbulent flow characteristics and heat transfer mechanism were discussed.

The different combinations of gas–liquid two-phase flow result in different flow patterns which is one of the most important flowing parameters in two-phase flow, and there are significant differences for flow characteristic and heat transfer in different flow patterns. In our previous investigations [23], a prediction model of convection heat transfer coefficient in oil cooling gallery was established, taking into consideration of several factors such as the structure of oil cooling gallery, physical properties of two-phase flow and characteristics of local flow in the cooling gallery under different piston diameters and engine speeds. In this paper, based on the experiment, the influence of oil injection pressures, liquid viscosities and diameters on the flow pattern distribution in the cooling gallery are studied by using the CFD software.

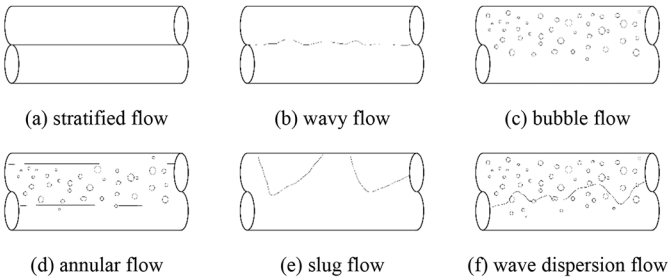

Fig. 1. Definition of flow pattern of two-phase flow in horizontal pipeline.

2 The definition of flow patterns

This paper mainly studies the flow pattern of the annular cavity of the cooling gallery. The fluid in the annular pipe is subjected to the gravitational force in vertical flow direction. In the static state, the liquid phase of larger density tends to locate at the bottom, so the definition of the gas–liquid two-phase flow in the horizontal pipeline can be referenced in the study. Compared with the vertical pipeline, the flow pattern in the horizontal pipeline is slightly complicated, and its flow pattern is divided into the following six categories and as shown in Figure 1.

Figure 1a shows the stratified flow. Generally, the heavier liquid phase flows in the lower part of the pipeline, while the gas phase flows in the upper part of the pipeline, and the two-phase interface is a relatively smooth horizontal plane.

Figure 1b shows a wave flow. The characteristic of the wave flow is that the interface of the gas–liquid phases can be clearly seen, but it is presented as a wave-shaped surface.

Figure 1c shows the bubble flow. Liquid phase fills the entire pipeline while bubbles disperse in the liquid medium, and a trend is presented in the upper part of the pipeline. Even in high-speed flow systems, the bubbles are evenly distributed and present in a foamy form.

Figure 1d shows the annular flow. This flow is generally divided into three layers where the upper and lower parts of the pipeline are liquid phase and the middle is the gas phase. The liquid phase is adhered to the tube wall, forming a liquid film, the distribution of which is not uniform. Besides, the liquid film near the bottom is thicker than that in the upper part. The gas phase in the middle is usually mixed with droplets.

Figure 1e shows the slug flow. A large bubble or a bullet-shaped bubble appears in the upper part of the pipe. When the gas volume fraction is important, the tip of the bubble is brought into contact with the surface of the tube wall and

Table 1. Technical parameters of internal combustion engine.

Items	Speed (test value) (r/min)	Speed (numerical value) (r/min)	Stroke (mm)	Length of connecting rod (mm)
Parameter	300–600	600–3000	144	216

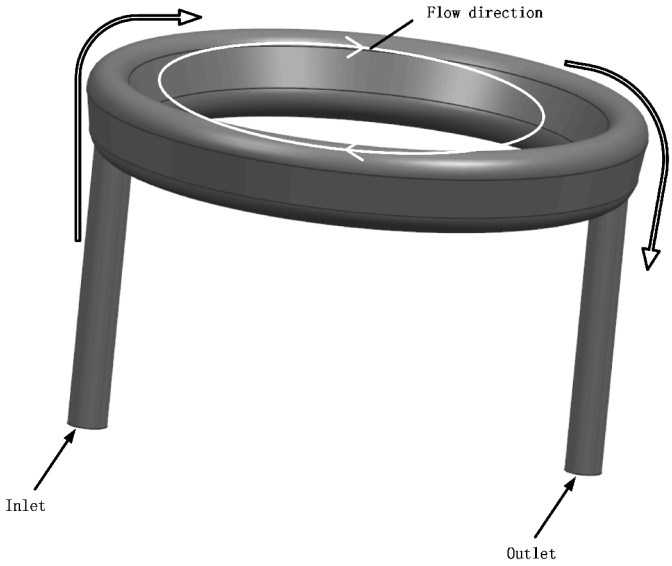

Fig. 2. The schematic diagram of internal cooling oil chamber.

is continuously separated from the liquid phase, forming a structure where the transition between the gas and liquid flow can be found alternately hence namely the slug flow.

Figure 1f shows a wave dispersion flow. As the liquid filling rate decreases, the gas phase increases and the gas phase in the upper part of the pipe is mixed with dispersed droplets. At this moment the bottom of the pipeline liquid less, gas–liquid interface shows irregular wave shape and the interface and the top of the wall without contact, the liquid phase will have many small bubbles. The undulating flow is also known as a "pseudo-bomb" flow.

3 Research object

The operation parameters of the internal combustion engine are shown in Table 1. The across-section of annular channel in cooling gallery is irregular with both inlet and outlet placed in opposite. The oil is injected and divided into two flow, running along the periphery direction, then collected and exhausted at the outlet, as shown in Figure 2. Considering the computation cost, the fluid domain at bottom of piston is simplified into a cylinder.

4 Test description and experiment process

4.1 Test description

The dynamic visualization test bench is shown in Figure 3a and the schematic diagram of the test principle is presented in Figure 3b. The test bench comprises the workbench, alloy cast iron liners, the crystal cylinder, the piston, the crystal cooling gallery, the drive motor, the control panel and the hydraulic station (oil circulation control system). To facilitate the precise injection of oil, the nozzle is provided with a regulating block which is movable on the workbench. The nozzle is connected to the hydraulic station through pipelines, and the nozzle axis is aligned with the inlet center line by moving the adjustment block. The alloy cast iron cylinder is located above the workbench where the piston is placed and driven by the motor and crankshaft above on the workbench. Alloy cast iron cylinder liner below is a crystal cylinder, a crystal cooling gallery in the crystal cylinder is connected to the piston through the fixed disc and threaded rod. To facilitate observing the processes during the reciprocating motion of piston and recording the two-phase flow patterns in the cooling gallery, the transparent cylinder liner and cooling gallery are fabricated by visual materials.

In addition, the dynamic visualization test bench contains a hydraulic station control panel for controlling the operating state of the hydraulic station and a motor control panel for controlling the operating state of the driving motor. In this way, with the different speeds of the piston, different temperatures and pressures of the injected oil flow can be observed clearly.

4.2 Experiment process

In the present study, due to the restrictions of the dynamic test bench conditions, only the visualization test with speed 600 r/min was carried out. The test procedure is as follows: (1) the piston is installed so that the piston is located at the bottom dead center (BDC, seen in Fig. 4) and the test tooling system is tested to verify that the distance between the nozzle and the oil inlet is the actual when piston operation. (2) Check the oil injection system, ensuring that the axes of nozzle and the inlet are in a line, in order to reduce the error caused by the test system; (3) start the cooling system to prevent the oil temperature is too high so as to ensure the normal operation of the fuel injection system; (4) start the hydraulic station and adjust the oil inject pressure through the control panel; (5) start the driving motor, and adjust the speed to 600 r/min and (6) record flow patterns through the high-speed camera during the test process.

5 Numerical simulation

5.1 Turbulence model

In this paper, FLUENT is employed to solve the problem of three-dimensional transient flow. According to the literature [18,19], the SST k–ω turbulence model is more accurate than the k-epsilon turbulence model in predicting

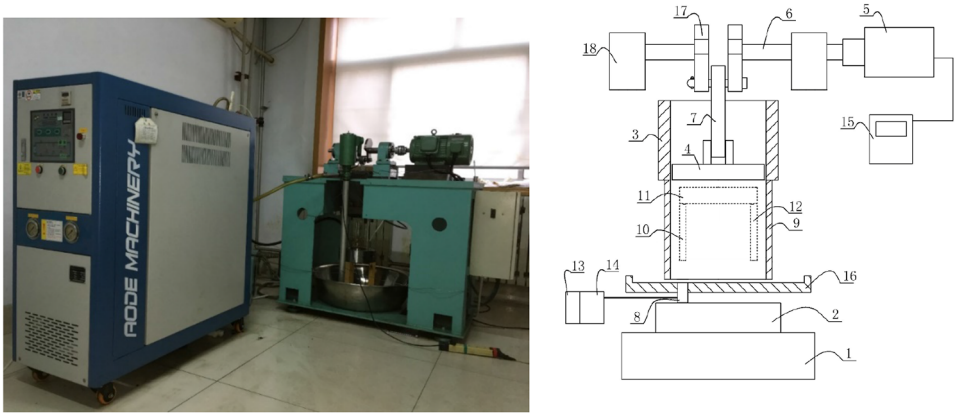

(a) (b)

Fig. 3. Visualization test system diagram. (a) Test setup. (b) Schematic diagram of the test: 1 – workbench, 2 – adjustment block, 3 – cylinder liner, 4 – piston, 5 – drive motor, 6 – crankshaft, 7 – connecting rod, 8 – nozzle, 9 – transparent glass cover, 10 – oil inlet pipe, 11 – annular cavity, 12 – oil outlet pipe, 13 – hydraulic station control panel, 14 – hydraulic station, 15 – motor control panel, 16 – oil pan, 17 – balance block, 18 – fixed platform.

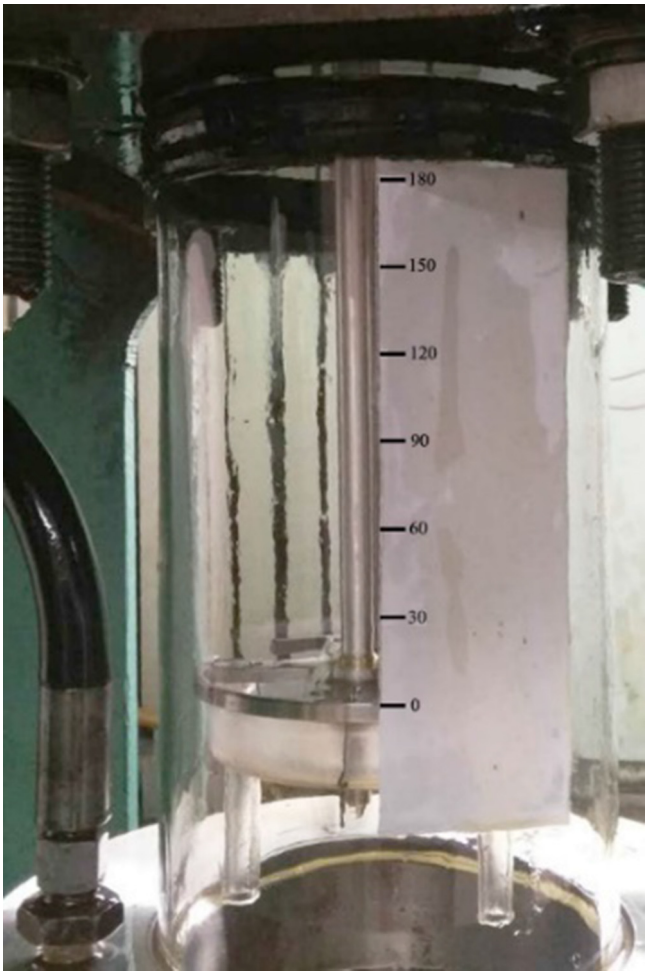

Fig. 4. The location of the cooling gallery.

the cooling effect. The core method is that the near-wall utilizes the robustness of the k–ω model to capture the flow of the viscous sublayer. However, the use of k-epsilon model in the mainstream can avoid the disadvantage of the k–ω model being too sensitive to the inlet turbulence parameters. The SST k–ω model is a two-equation model that combines the k–ω model with the k-epsilon model and expressed in equations (1) and (2).

$$\frac{\partial}{\partial t}(\rho k)+\frac{\partial}{\partial x_i}(\rho k u_i)=\frac{\partial}{\partial x_j}\left(\Gamma_k\frac{\partial k}{\partial x_j}\right)+\tilde{G}_k-Y_k+S_k \quad (1)$$

$$\frac{\partial}{\partial t}(\rho\omega)+\frac{\partial}{\partial x_i}(\rho\omega u_i)=\frac{\partial}{\partial x_j}\left(\Gamma_\omega\frac{\partial \omega}{\partial x_j}\right)+G_\omega-Y_\omega +D_\omega+S_\omega \quad (2)$$

In the equation, G_k is the production phase of the turbulent kinetic energy due to the average velocity gradient and G_ω is the generating phase of ω. Γ_k and Γ_ω represent the effective diffusion coefficients of k and ω, respectively. Y_k and Y_ω denote the turbulent dissipative phases of k and ω, respectively. D_ω represents the orthogonal diffusion term. S_k and S_ω are self-defined sources.

Turbulent kinetic energy k and ω are respectively calculated by equations (3) and (4).

$$k=\frac{3}{2}(w\cdot I)^2 \quad (3)$$

$$\omega=\frac{k^{1/2}}{C_\mu^{1/2}l} \quad (4)$$

where u is the average velocity, I is the turbulence intensity and C_μ is the empirical constant and assigned to 0.09 by default.

5.2 Two-phase flow model

As there are various factors affecting the interface of the two-phase flow in cooling gallery, the flow field, especially the density and viscosity of flow field contribute to the

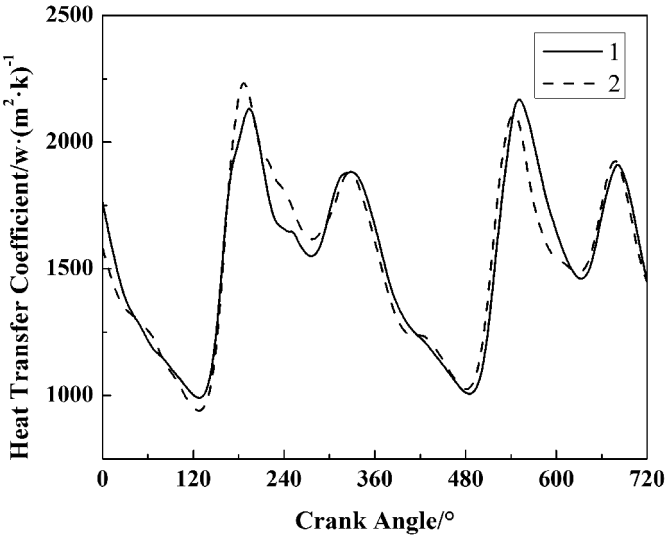

Fig. 5. The comparison of heat transfer coefficients.

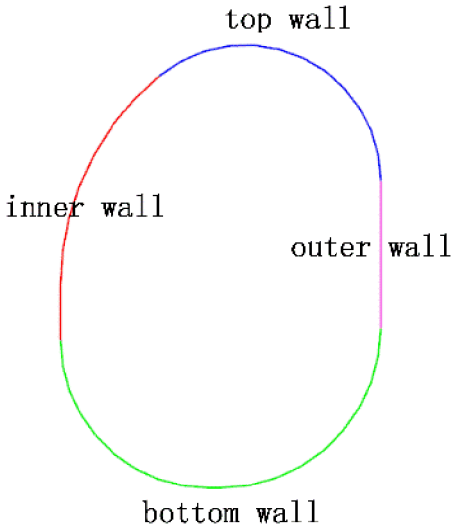

Fig. 6. The schematic diagram of the area zones of cooling gallery.

variation of the position and surface shape of interface significantly. In addition, the phase interface is the transmission channel of mass, momentum and energy between gas and liquid phases. Therefore, the accurate tracking of the phase interface is essential in solving the governing equations.

In this paper, the Level-set + VOF (volume of fluid) coupling model is established to solve the same momentum equations for gas–liquid two-phase flow wherein the VOF equation is considered as the main body, and the level set function is employed to correct the normal direction of the interface instead of that in the VOF model (represented by n). The two-phase flow is simulated by tracking the volume fraction of gas and liquid phases. Comparing with CLSVOF mentioned in reference [21], the process of repeated initialization of Level-set is omitted in the Level-set + VOF coupling model which is similar to the CVOFLS model mentioned in [24]. The Level-set + VOF coupling model directly applies the generated linear interface to the interface correction of the VOF model leading to improvements of accuracy and time efficiency of the calculation. Furthermore, the clarity of the two-phase interface is also improved. The choose of the explicit–implicit approach simply refer to the literature or the Fluent manual.

In addition to terms of convection and viscosity, there is amount of volumetric forces (such as gravity or surface tension) existing in the two-phase flow of cooling gallery thus the body force and pressure gradient terms in the momentum equation are in an equilibrium state. Due to the local balance of pressure gradient and body force, the separation algorithm converges poorly. The implicit force in FLUENT is used to improve the convergence of solutions, considering the partial equilibrium of pressure gradient and body force in the momentum equation. Figure 5 compares the heat transfer coefficients by using implicit volume forces and that without using implicit volume forces. As in the figure, curve 1 represents the activation of the implicit volume force while curve 2 illustrates the closure of the implicit volume force. It can be seen that the use of implicit volume force can effectively reduce the instability of the calculation results.

5.3 Boundary conditions

(1) The velocity inlet boundary conditions are employed and expressed as

$$w = w_{\text{in}}, u = v = 0 \tag{5}$$

$$T = T_{\text{in}} = 393\,\text{K}. \tag{6}$$

(2) The pressure outlet boundary conditions are adopted and expressed as

$$p = p_{\text{atm}} \tag{7}$$

$$\frac{\partial T}{\partial n} = \frac{\partial k}{\partial n} = \frac{\partial \omega}{\partial n} = 0. \tag{8}$$

(3) Wall boundary conditions

The cooling gallery is divided into four area zones, as shown in Figure 6. The wall temperature of each zone is set according to the actual temperature of piston cooling gallery. And no-slip boundary condition is applied in the calculation.

(4) Surface tension boundary conditions are defined as follows

$$p_2 - p_1 = \sigma\left(\frac{1}{R_1} + \frac{1}{R_2}\right) \tag{9}$$

$$n = \nabla\alpha_{\text{oil}}/|\nabla\alpha_{\text{oil}}| \tag{10}$$

$$\rho_k = \nabla \cdot n \tag{11}$$

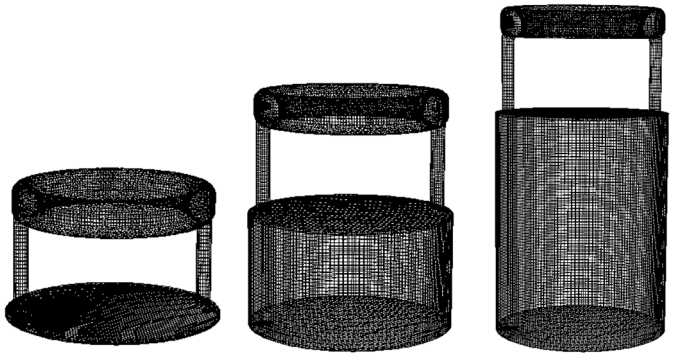

Fig. 7. Schematic of mesh model in fluid domain of cooling gallery.

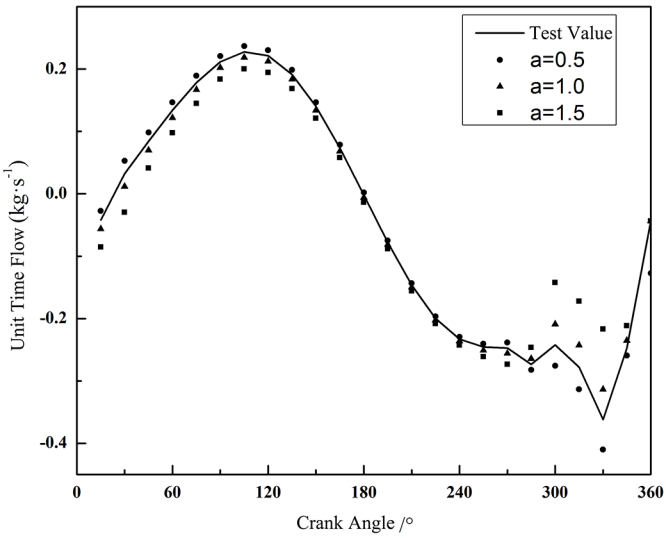

Fig. 8. Effect of dynamic mesh refinement on the outlet flow of cooling gallery.

where σ represents the surface tension coefficient while R_1 and R_2 are the curvature radius of the liquid surface on the two perpendicular surfaces. ρ_k denotes the curvature radius of the plane and the surface tension can be written in terms of the pressure jump across the surface refer to the literature or the Fluent manual.

5.4 Analysis of mesh accuracy

The mesh generation is considered as an important process during the pre-processing of numerical calculation. The reciprocating motion of piston is simulated by dynamic mesh model, neglecting the lateral motion of piston. Under assumption that only the rigid motion is expected to occur in the entire fluid region, the dynamic mesh-based model is established as shown in Figure 7. The density of mesh is adjusted by changing the mesh size in the way of which the dynamic grid size is assigned to 0.5, 1.0 and 1.5 ratio of surrounding grid size. The inlet flow of cooling gallery is obtained by calculation then compared with the test results. In this procedure, the effect of grid accuracy on the results can be analyzed.

Figure 8 illustrates the effect of grid densification on the flow of cooling gallery Q_{out}. It can be seen that the deviations between numerical results and test data concerning different ratios all drop in an appropriate range of 10% which is acceptable in industrial applications. Results show that the mesh refining affects the accuracy of computational results. When the ratio between dynamic mesh size and surrounding mesh size a varies in the range of 0.5–1.0, a higher accuracy can be obtained. As a result, the ratio $a = 1.0$ is selected hence the dynamic mesh size is 2 mm for its moderate computation time and relatively high accuracy.

6 Results and discussion

6.1 Comparison of numerical results with experimental results

The numerical simulation of the two-phase flow in cooling gallery under an engine speed of 600 r/min was performed. Results are compared with the visualization test, selecting the flow pattern of the key position, such as the top dead center (TDC) during the operation of the piston, and are shown in Table 2.

When cooling gallery reaches the BDC, the oil impacts the bottom of the cooling gallery and accumulates in the bottom when the cooling gallery changes its direction of movement, showing obvious stratified flow patterns combined with oil drops. Meanwhile, the quantity of oil flowing out of the cooling gallery becomes greater. As the cooling gallery continues to move upward, most of the oil is still accumulated at the bottom of the cooling gallery due to its inertia. When the cooling gallery moves to the point where the crank angle is close to 90°, the oil starts to separate from the bottom of the cooling gallery, further a relatively stable flow pattern is formed by two-phase flow when the crank angle reaches 90°. In subsequent upward motion of the cooling gallery, the oil impacts the wall upwardly. Likewise, when the cooling gallery reaches the TDC, the oil almost accumulates on the top of the cooling gallery under the action of inertia and little oil outflow can be observed at the outlet of the cooling gallery. Then the cooling gallery continues to descend and the direction of oil acceleration changes, pushing the wall of cooling gallery downward. When the cooling gallery corresponds to 270° of the crank angle, the oil begins to separate from the surface of the upper wall, and the flow pattern of the two-phase flow in the cooling gallery changes simultaneously. The shape of the wave flow is in the opposite direction to the flow at 90° of crank angle.

The comparative results show a good agreement between the numerical results with the flow pattern obtained from the visualization test. Therefore, the numerical method is verified to be reliable and accurate to simulate the two-phase flow process of cooling gallery.

Table 2. Comparison of numerical simulation results and test results of flow pattern in cooling gallery.

Crank angle	30°	90°
Visualization test results	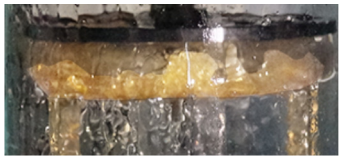	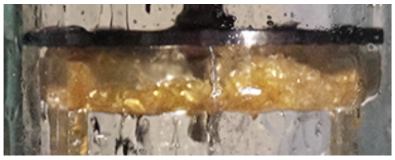
Umerical simulation results	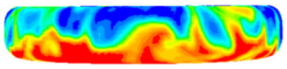	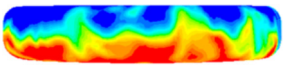
Crank angle	TDC	270°
Visualization test results	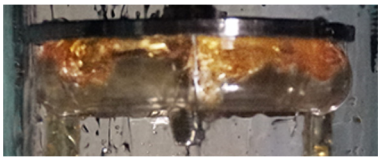	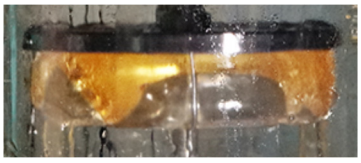
Numerical simulation results	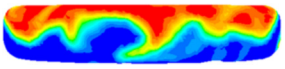	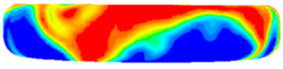

6.2 Influence of engine speed on flow pattern of two-phase flow

The oscillations of the oil in the cooling gallery are predicted by the numerical model under rotational speeds of 600 r/min, 1500 r/min and 2000 r/min. The results concerning the key position are illustrated in Table 3. The profiles of gas–liquid interface reveal that the higher the engine speed, the more obvious oscillation characteristics are. Before reaching the TDC, the distance between the nozzle and the inlet of oil cooling gallery increases, the fill ratio of the cooling gallery decreases and the shape of wave segment increases. And with the rise in the location of the cooling gallery, the formation of the wave position of the oil forward, from the crankshaft angle of 90°, the formation of the wave position of oil backward shift. As the fluctuation range increases with the crankshaft angle, the "liquid plug" phenomenon is more likely to occur (such as $\alpha = 150°$). After reaching the TDC, the coverage of the liquid back to the lower wall increases and the peak direction changes.

As shown in Figure 9, the increase of the engine speed results in the rise of difference between the cooling gallery and the oil injection speed, and leads to the decrease of the amount of oil entering the internal cooling oil chamber per unit time. However, the increase of engine speed contributes to increase of the oil oscillation intensity hence the oil coverage. When the engine speed is small, the amplitude of the oil in the cooling gallery is relatively small thus the erosion of the wall is weakened, and the heat transfer intensity is also reduced. Increasing engine speed leads to the increase of instantaneous impact speed while the oil rushes to both the top and bottom at the inside of the cooling gallery which, however, plays key role in enhancing the heat transfer. As a result, the increase of engine speed results in increase of the heat transfer coefficient. It also can be seen from the Figure 9 that the lower the engine speed, the smaller the variation range of the heat transfer coefficient. The results indicate that the engine speed affects the distribution of the heat transfer coefficient significantly.

6.3 Influence of liquid viscosity on flow pattern of two-phase flow

It is worth to note that the viscosity of the oil–gas two-phase flow affects the flow significantly. Table 4 compares the flow patterns of fluids with different viscosities and locations. It is shown that as the piston reciprocates, waves in different amplitudes are formed irregularly at the gas–liquid interface in forms of segments. Some waves move a short distance and then disappear while some waves move the crest height which. Besides, the wave length is variable. As the liquid temperature rises, the viscosity decreases and then tends to be consistent whereas the liquid surface movement of small waves tends to be stable. When the piston arrives at the BDC or TDC, some waves are blocking the entire pipe cross-section, and the slug flow is formed. After the TDC, the liquid viscosity decreases and the gas–

Table 3. Variation of flow patterns of two-phase flow under different speeds.

Crank angle	600 r/min	1500 r/min	2000 r/min
BDC	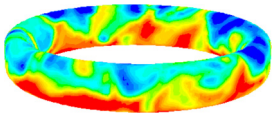	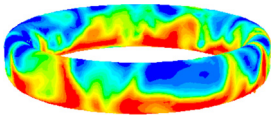	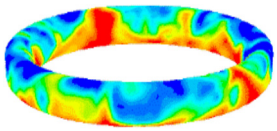
60°	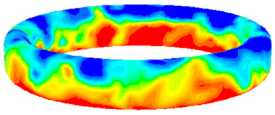	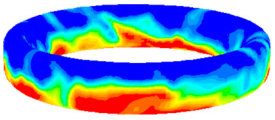	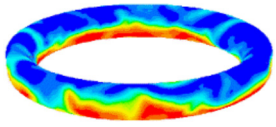
120°	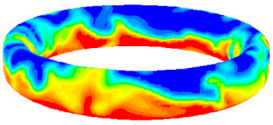	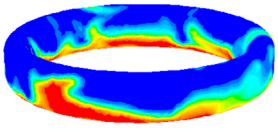	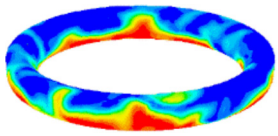
TDC	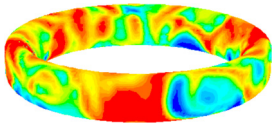	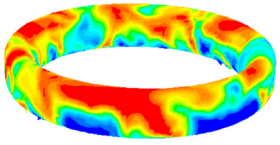	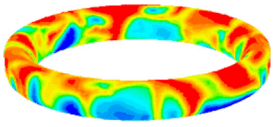
240°	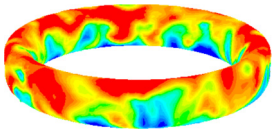	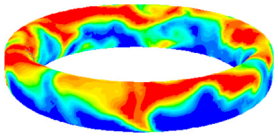	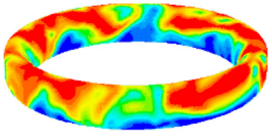
300°	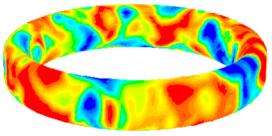	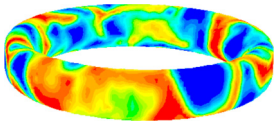	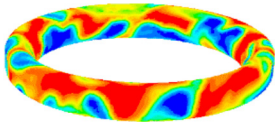

liquid interface is more likely to be prone to fluctuate. The smaller the viscosity, the more the locations of the slug flow appears at and the more oil that enters into the "liquid plug" section contributing to frequent occurrence of the slug flow.

Figure 10 illustrates the kinematic viscosity of the oil at temperatures of 110 °C (a), 85 °C (b), 75 °C (c) and 65 °C (d), respectively. Results show that liquid viscosity has a great effect on the oil coverage and the heat transfer coefficient related to the fact that the decrease of oil viscosity leads to the increase of oil coverage. The smaller the viscosity of the oil, the more oil "thin", the easier the oil film to be formed, and larger amount of small oil droplets are distributed in the internal cold oil chamber, attached to the wall with the cooling gallery reciprocating movement hence less amount of oil is participated in oscillation. Therefore, it is opposite to the changing laws of oil coverage, with the increasing of oil viscosity, more oil is involved in the oscillation and more "plugs" are generated in cooling gallery. At the same time, the oil impacts the wall with higher speed, so the convection heat transfer coefficient increases, and more heat is taken away through it. In Figure 10b, it can also be seen that as the viscosity decreases, the oil flows slowly, and the peak heat transfer coefficient tends to "backward".

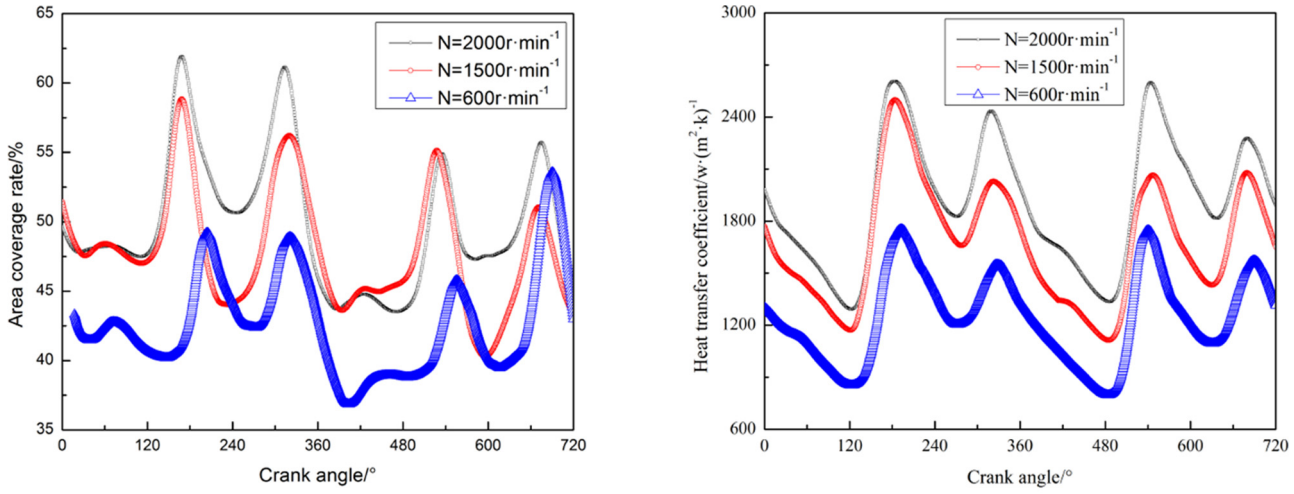

(a) Area coverage of the cooling gallery (b) Wall heat transfer coefficient

Fig. 9. The change of area coverage and heat transfer coefficient under different speeds.

Table 4. Variation of flow patterns of two-phase flow under different liquid viscosities.

Crank angle	a	b	c	d
BDC				
60°				
120°				
TDC				
240°				
300°				

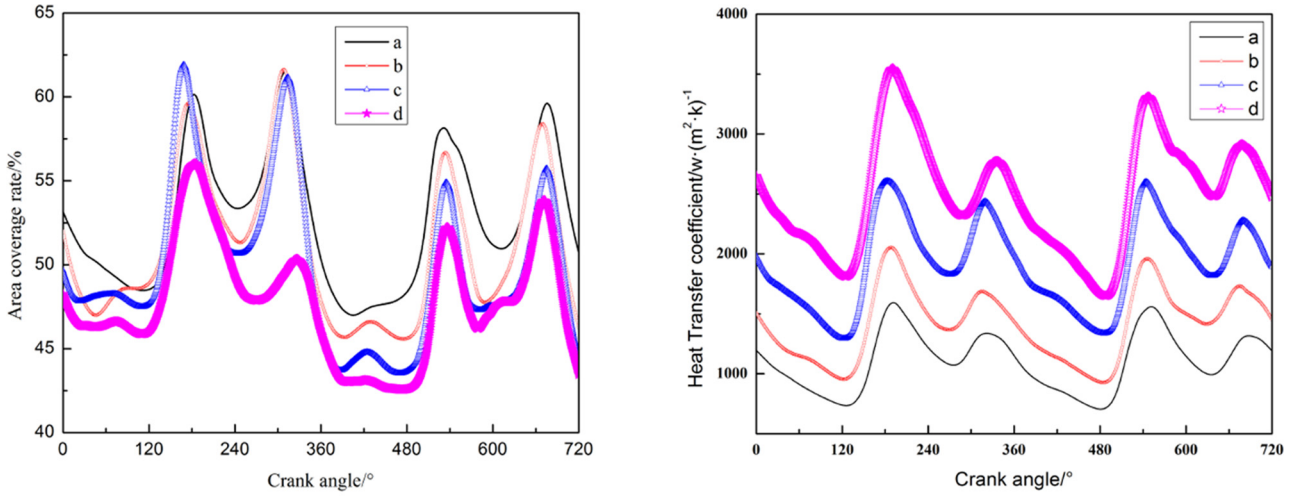

(a) Area coverage of the cooling gallery (b) Wall heat transfer coefficient

Fig. 10. The change of area coverage and heat transfer coefficient under different liquid viscosities.

Table 5. Variation of flow patterns of two-phase flow under different injection pressures.

Crank angle	$P = 4.5$ bar	$P = 3.0$ bar	$P = 2.0$ bar
BDC			
60°			
120°			
TDC			
240°			
300°			

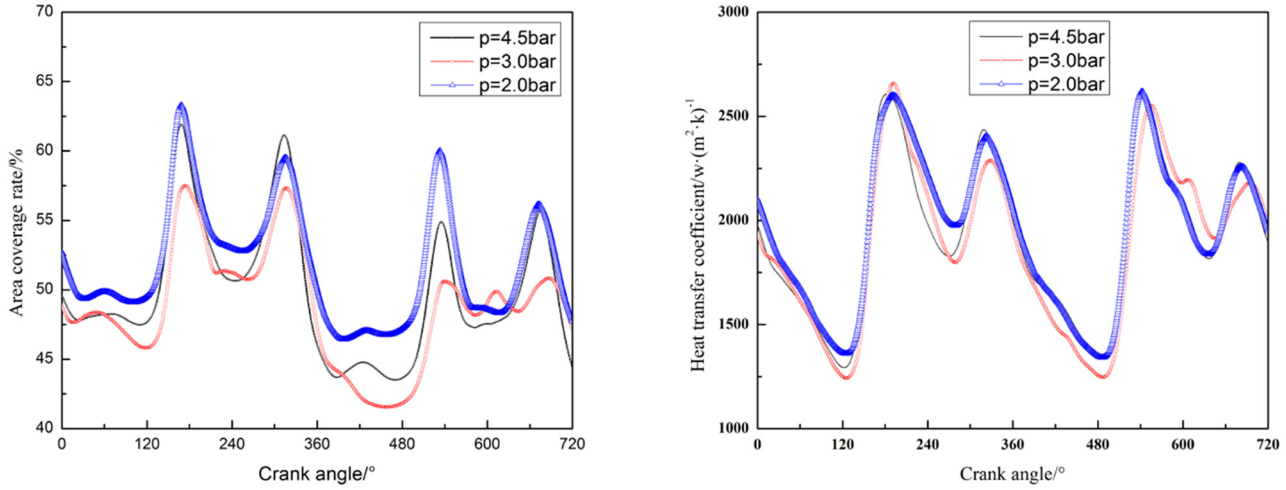

(a) Area coverage of the cooling gallery (b) Wall heat transfer coefficient

Fig. 11. The change of area coverage and heat transfer coefficient under different injection pressures.

It can be summarized that the viscosity is an important factor affecting the change of the two-phase flow pattern in the cooling gallery. As the turbulence intensity of the liquid is different, the oscillation frequency of the liquid is different, the gas–liquid interface changes, resulting in the flow pattern distribution and the wall heat transfer coefficient change.

6.4 Influence of injection pressure on flow pattern of two-phase flow

Table 5 shows the variation of the two-phase flow patterns in the cooling gallery under different injection pressures. It is found that the distribution of the injection pressure has little effect on the distribution of convective flow. Under the action of the reciprocating motion of piston, the flow pattern alternates within the wave flow and the slug flow. While engine speed is constant, the increase of the injection pressure leads to the increase of the relative velocity as well as the acceleration of the two-phase flow in the internal cooling oil chamber so that the maximum amplitude and the position of the liquid plug are slightly moved. By contrast, the decrease of the oil injection pressure contributes to the reduction in fluctuation of the two-phase flow and the increase of the plug length.

The effect of oil injection pressure on the filling ratio and heat transfer coefficient is faint as well, as shown in Figure 11. Under the same operating conditions, as the injection pressure increases, an increase can be obtained in jetting speed of the nozzle, the relative velocity of the internal cooling chamber, the nozzle injection and the oil output with corresponding fill ratio increased as well. In addition, oil injection pressure has little impact on heat transfer coefficient of the oil cooling wall. The oil coverage is too high so that the oscillation intensity of liquid in the cooling gallery is weakened, inducing that the heat transfer coefficient reduces and piston cooling effect is proved to be not good.

6.5 Influence of pipe size on the flow pattern of two-phase flow

The variation of the cooling gallery can be achieved by changing the cross-sectional area of the pipe. Table 6 shows that the change of the diameter of the pipe has little effect on the overall distribution of the flow pattern; however, the influence of which is significant on the boundary of the convective transition. To be more exact, when the characteristic diameter of the cooling gallery is expanded, the length of wave flow keeps to be longer, followed by transition of the critical point of the flow pattern. Likewise, when the inner diameter of the cooling gallery becomes larger, the oscillation appears to be more intense and occurrence of the slug flow formation becomes more frequent with the length of the plugs becoming shorter.

Figure 12 shows the dependency of the oil coverage and wall heat transfer coefficient on different cooling galleries. Increasing the cooling gallery in a certain range leads to the increase of the oil coverage and the diameter. Moreover, the movement of the oil turbulence in the cooling gallery becomes more intense resulting into a continuous collision with the wall hence to erosive wear. Meanwhile, the interaction between the axial flow and the circumferential flow is expected to be more obvious. The plug is subjected to vary under the action of the shear flow, which increases the heat transfer coefficient so as to the heat transfer performance.

7 Conclusions

The effect of the two-phase flow pattern on heat transfer of cooling gallery is investigated where the numerical model based on CFD is presented and a good agreement is obtained between the prediction results and the visualization tests. Conclusions can be summarized as follows:

(1) The CFD method is verified to be a feasible approach in simulating the two-phase flow of piston

Table 6. Variation of flow pattern of two-phase flow under different diameters.

Crank angle	He = 16 mm	He = 18 mm	He = 20 mm
BDC	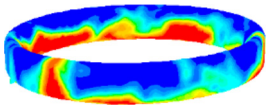	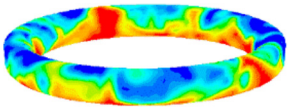	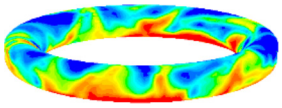
60°	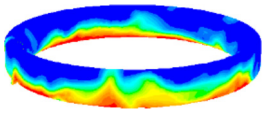	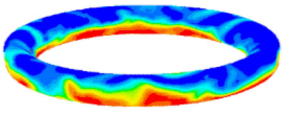	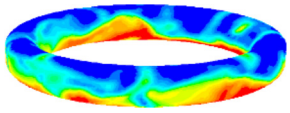
120°	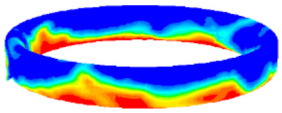	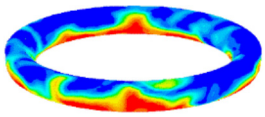	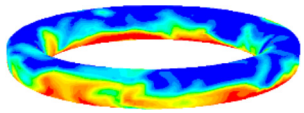
TDC	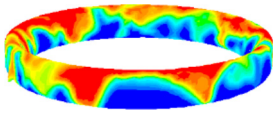	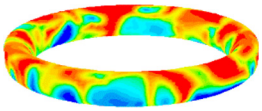	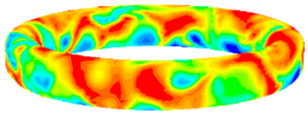
240°	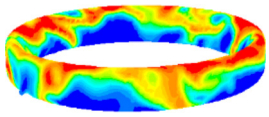	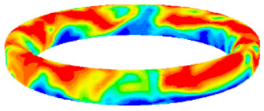	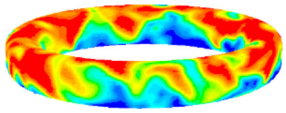
300°	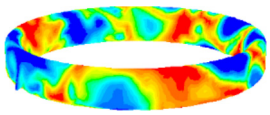	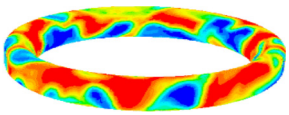	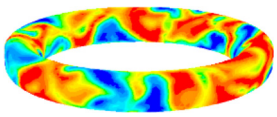

cooling gallery. The wave flow and slug flow are proved to be the main flow patterns of the two-phase flow in the cooling gallery. During the reciprocating motion of piston, the length of the wave flow and the length of the slug flow are unstable, and the height of the amplitude is also different. It is also revealed that the oil injection pressure has little effect on the overall distribution of the flow pattern and heat transfer coefficient. The engine speed, liquid viscosity and cooling gallery size are identified to be the primary factors influencing the two-phase flow patterns of the cooling gallery.

(2) At a lower engine speed, the two-phase flow in the cooling gallery is dominated by the undulating flow. As the engine speed increases, the "liquid plug" phenomenon becomes more obvious. The increase of engine speed results in the enhancement of oil oscillation as well as the complexity of two-phase flow patterns in the cooling gallery. Besides, when the engine speed increases, the oil speed in washing the wall also increases, inducing the increase of the heat transfer coefficient.

(3) When the liquid viscosity decreases, gas–liquid interface is more likely to be prone to fluctuate. The smaller the viscosity, the more the oil entering into the liquid plug, resulting in the decrease of slug flow in height. Meanwhile, the occurrence of slug becomes frequent and turbulence intensity increases, leading to the increase of heat transfer coefficient hence the enhancement of the heat transfer performance.

(4) The cross-sectional size of the cooling gallery has a significant effect on the flow pattern of the two-phase flow. Increasing the intrinsic diameter of the cooling gallery enables the oscillation of the two-phase flow to be more

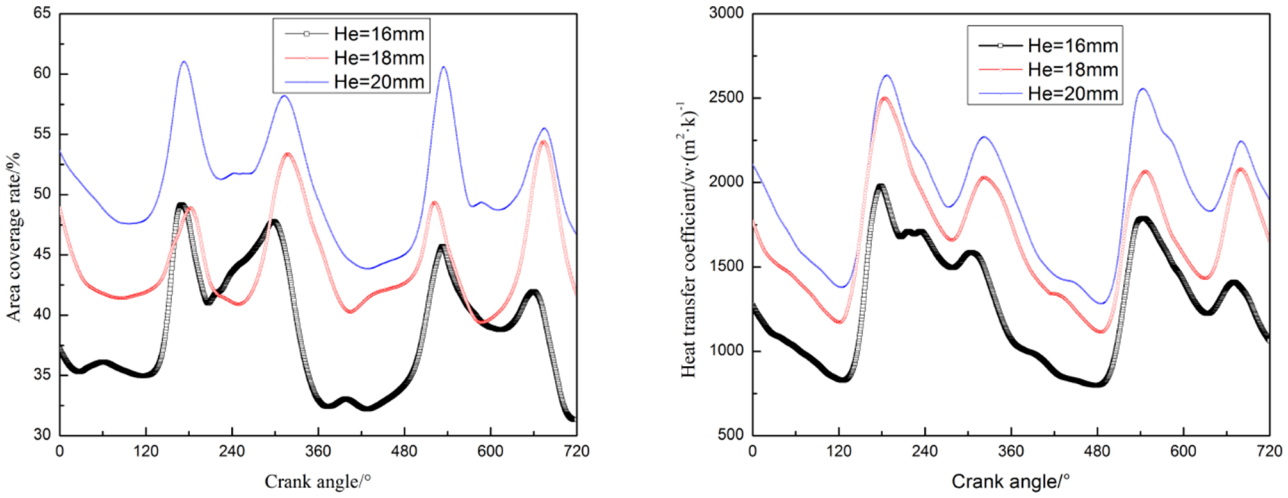

(a) Area coverage of the cooling gallery (b) Wall heat transfer coefficient

Fig. 12. The change of area coverage and heat transfer coefficient under different diameters.

intense. The flow pattern changes more frequently and the length of the slug flow becomes shorter while the heat transfer coefficient increases.

Acknowledgement. This research is supported by National Natural Science Foundation of China (Grant No. 51705028); Natural Science Foundation of Shandong Province (Grant No. ZR2016EEB36); Scientific Research Project of Colleges and Universities of Shandong Province (Grant No. J17KA025), Research Funding of Binzhou University (Grant No. BZXYZZJJ201703) and PhD Research Funding of Binzhou University (Grant No. 2018Y12).

References

[1] D.C. Luff, T. Law, P.J. Shayler et al., The effect of piston cooling jets on diesel engine piston temperatures, emissions and fuel consumption, SAE Int. J. Engines 5 (2012) 1300–1311
[2] H.R. Zhu, W.Z. Zhang, Y.P. Yuan, Study on oscillating cooling effect of hightly-intensified piston considering turbulence model difference, Chin. Intern. Combust. Engine Eng. 37 (2016) 78–82
[3] Mahle GmbH, Pistons and Engine Testing, Vieweg Teubner Verlag, Wiesbaden, 2011
[4] A.J. Torregrosa, A. Broatch, P. Olmeda, N.J. Martı, A contribution to film coefficient estimation in piston cooling galleries, Exp. Therm. Fluid Sci. 34 (2010) 142–151
[5] A.J. Torregrosa, P. Olmeda, B. Degraeuwe, M. Reyes, A concise wall temperature model for DI diesel engines, Appl. Therm. Eng. 26 (2006) 1320–1327
[6] C.A. Evans, Cocktail Shaker, Heat Transfer Science Library, University of Nottingham, 1977
[7] M. Pimenta, R. Filho, Cooling of automotive pistons: study of liquid-cooling jets, SAE Technical Paper 931622, 1993
[8] N. Yu, T. Yamada, Y. Takeuchi, K. Akimoto, Development of techniques for improving piston cooling performance (first report)-measurement of heat absorption characteristics by engine oil in cooling channel, SAE Technical Paper, 2005-08-0372
[9] Y. Takeuchi, K. Akimoto, T. Noda, Y. Nozawa, T. Yamada, Development of techniques for improving piston cooling performance (second report)-oil movement and heat transfer simulation in piston cooling channel with CFD, SAE Technical Paper, 2005-08-0373
[10] H. Kajiwara, Y. Fujioka, T. Suzuki, H. Negishi, An analytical approach for prediction of piston temperature distribution in diesel engines, JSAE Rev. 23 (2002) 429–434
[11] H. Kajiwara, Y. Fujioka, H. Negishi, Prediction of temperatures on pistons with cooling gallery in diesel engines using CFD tool, SAE Technical Paper, 2003
[12] W.S. Fu, S.H. Lian, L.Y. Hao, An investigation of heat transfer of a reciprocating piston, Int. J. Heat Mass Transf. 49 (2006) 4360–4371
[13] J.F. Pan, Nigro Roberto, Matsuo. Eduardo, 3-D modeling of heat transfer in diesel engine piston cooling galleries, SAE Paper 2005-01-1644
[14] Y. Yong, M. Reddy, M. Jarrett, C. Kinsey, CFD modeling of the multiphase flow and heat transfer for piston gallery cooling system, SAE Technical Paper, 2007
[15] P. Hanafizadeh, A. Hojati, A. Karimi, Experimental investigation of oil-water two phase flow regime in an inclined pipe, J. Petrol. Sci. Eng. 136 (2015) 12–22
[16] X. Deng, J. Lei, J. Wen et al., Numerical investigation on the oscillating flow and uneven heat transfer processes of the cooling oil inside a piston gallery, Appl. Therm. Eng. 126 (2017) 139–150
[17] J. Wang,Research on the Dynamic Behavior of Gas-Liquued Two-Phase Flow, Shanghai Jiao Tong University Press, Shanghai, 2012
[18] Y.P. Liu, Study on the Flow Regime Transition in Horizontal Gas-Oil Flow and the Characteristics of Gas-Liquid Interface, Shanghai Jiao Tong University, Shanghai, 2008
[19] R. Kong, S. Kim, S. Bajorek et al., Effects of pipe size on horizontal two-phase flow: flow regimes, pressure drop, two-phase flow parameters, and drift-flux analysis, Exp. Therm. Fluid Sci. 96 (2018) 75–89
[20] J. Lu, P. Wang, M. Bai, J. Li, K. Zeng, Experimental visualization of gas-liquid two-phase flow during reciprocating motion, Appl. Therm. Eng. 79 (2015) 63–73

[21] P. Wang, J. Lv, M. Bai, K. Zeng, The reciprocating motion characteristics of nanofluid inside the piston cooling gallery, Powder Technol. 274 (2015) 402–417
[22] P. Wang, K. Han, S. Yoon et al., The gas-liquid two-phase flow in reciprocating enclosure with piston cooling gallery application, Int. J. Therm. Sci. 129 (2018) 73–82
[23] Z. Jian, D. Lijun, L. Shiying et al., Steady heat transfer prediction model for oil cooling gallery in the piston of internal combustion engine, Trans. CSICE (2018)
[24] W. Zhou, Y. Ou, L. Cui A coupled volume of fluid and level set (CVOFLS) method for tracking moving interfaces, Chin. J. Eng. Math. 32 (2015) 697–708

Cite this article as: L. Deng, J. Zhang, G. Hao, J. Liu, Numerical and experimental investigation on the effect of the two-phase flow pattern on heat transfer of piston cooling gallery, Mechanics & Industry **20**, 507 (2019)